Bleaching-resistant single-molecule fluorescence and FRET monitoring based on fluorophore exchange via transient DNA binding

Mirjam Kümmerlin[a,b], Abhishek Mazumder[a,b], and Achillefs N. Kapanidis[a,b,*]

[a] Biological Physics Research Group, Clarendon Laboratory, Department of Physics, University of Oxford, Oxford OX1 3PU, United Kingdom

[b] Kavli Institute for Nanoscience Discovery, New Biochemistry Building, University of Oxford, South Parks Road, Oxford, OX1 3QU, United Kingdom

*To whom correspondence should be addressed. Tel: +44-1865-272-226; Email: kapanidis@physics.ox.ac.uk.

ABSTRACT

Photobleaching of fluorescent probes limits the observation span of a typical single-molecule fluorescence measurement and hinders simultaneous observation of dynamics across timescales. Here, we present a general strategy to circumvent photobleaching by replenishing fluorescent probes throughout the experiment via transient binding of fluorescently labelled single-stranded DNAs to complementary target DNA strands attached to the target molecule. We show our strategy allows observation of near-continuous single-molecule fluorescence for more than an hour, a timescale two orders of magnitude longer than the photobleaching time under our conditions. We also show our method is adaptable to FRET and study the conformational dynamics of DNA Holliday Junctions for extended periods. By adjusting the temporal resolution and observation span, we envision capturing the conformational dynamics of proteins and nucleic acids over a wide range of timescales.

INTRODUCTION

Single-molecule methods have transformed the study of biological systems by enabling detailed interrogation of the structure, dynamics, and function of individual molecules. These methods offer unique insight into a wide range of biological molecules and processes, including the assembly and folding of proteins, the mechanisms of gene expression and maintenance, the structure-function relationships of molecular assemblies, and the coupling of large macromolecular machines, both in vitro and in vivo.[1]

In particular, single-molecule fluorescence (SMF) spectroscopy and microscopy studies have been very popular, since they are sensitive, versatile, and compatible with living cells.[2] Some SMF studies involve labelling the biomolecule of interest with a single fluorophore[3], which allows detection of the presence of the labelled molecule, and localisation of its position with high precision. These capabilities in turn enable measurements of molecular stoichiometries, as well as super-resolution imaging and single-molecule tracking.[4–10] Other SMF studies involve single-molecule fluorescence resonance energy transfer (smFRET), which typically uses two complementary fluorophores to monitor distances in the 2-10 nm range and can be used as a molecular ruler.[11,12] In addition to structural analysis, smFRET can report on the kinetics of conformational changes and relative motions of interacting species, which helps to deduce the sequence of events in many biological processes.[13]

Despite its advantages, most SMF methods are still severely limited by photobleaching, which is the irreversible photo-destruction and loss of signal of the fluorescent probes (either organic dyes or fluorescent proteins) used to label the biomolecules of interest; notably, the limitations caused by photobleaching have been evident since the early days of SMF.[2,14] Use of fluorescence stabilisation systems (such as oxygen scavengers and triplet-state quenchers) during *in vitro* experiments have significantly increased the lifespan of SMF-compatible fluorophores, but cannot permanently prevent photobleaching and other types of photodamage.[15] The current state-of-the-art means that typical observation spans for SMF extend from the low-second to the low-minute timescale.[16,17]

As a result of photobleaching, the photon budget per fluorophore (i.e., the number of photons emitted before the end of the observation) remains limited. Extension of the observation span of a specific experiment is possible by lowering laser excitation powers; however, this approach decreases the signal-to-noise ratio (SNR) of the measurement. The lower excitation power can be combined with a slower frame rate to recover the SNR, but this approach sacrifices salient dynamic information present at faster timescales.

A possible way to overcome photobleaching-driven limitations is to exchange the fluorescent labels during an ongoing experiment. This could be achieved using transient or reversible interactions between the target molecule (i.e., the molecule under study) and the fluorophore, provided that the system allows for an exchange of an attached fluorescent probe with a new probe *before* the attached probe gets

photobleached. To provide a simple analogy, we aim to replace our "single-molecule fluorescent light bulb" before it burns out to guarantee a constant supply of fluorescent light from the target molecule.

Transiently binding fluorophores have been used before to study targets for extended periods, especially in single-molecule localisation microscopy. An early and powerful example of such microscopy is the method of Points Accumulation for Imaging in Nanoscale Topography (PAINT)[16], where vesicles and lipid bilayers are imaged via the repeated transient binding of either an environmentally sensitive fluorophore or a fluorescently labelled protein. Along the same lines, DNA-PAINT achieved super-resolution via transient binding of short, labelled DNA strands ("imagers") to complementary "docking strands" on target biomolecules such as DNA nanostructures[17] and proteins.[18] Exchanging fluorescent labels has also been combined with stimulated emission depletion (STED) microscopy to enhance photo-stability.[19]

In these methods, the experimental conditions are tuned to ensure the presence of extensive "dark intervals" (i.e., time intervals where the target is not bound by a transient label, and thus is not fluorescent), since the temporal separation of single-molecule fluorescence signals from a diffraction-limited area is an absolute requirement for high-precision localisation and generation of a super-resolved image. As such, methods such as PAINT and DNA-PAINT cannot provide the *continuous* signal needed to monitor closely the presence or motions of a molecular target over extended observation spans.

In principle, the dark interval between the binding of two transient labels to the same target can be decreased by increasing the rate of binding, which in turn can be achieved either by increasing the transient label concentration, or by changing the properties of the transient label to increase the on-rate constant or both. However, the concentration of fluorescent transient labels cannot be increased much above 30 nM, as unbound labels contribute to the fluorescence background and degrade the SNR of the measurement[20–23], and this concentration will not allow for a high enough on-rate of short ssDNAs for continuous fluorescence traces.

Here, we introduce a DNA-hybridisation-based approach that optimises the label exchange to enable near-continuous, bleaching-free single-molecule fluorescence observations via **Re**newal of **F**luorescence via **Re**peated **s**sDNA **H**ybridisation (REFRESH, Figure 1A). We also extend this approach to smFRET (REFRESH-FRET, Figure 1B). The target biomolecule is modified with a short ssDNA docking strand that is recognised by a complementary DNA carrying a fluorophore; we will use the term "renewable label" ("r-label") for the DNA-fluorophore conjugate (as opposed to "transient label", since the latter implies very short binding events to the target, which is not the case in our method). The design involves optimising the hybridisation kinetics to minimise dark intervals and enable continuous (or near-continuous) emission of fluorescence from a target biomolecule with both high temporal resolution and extended observation span (>1 hr, Figure 1A, bottom). We show that we can specifically label a domain within a molecule which is also covalently labelled with a complementary fluorophore and enable smFRET measurements. Finally, we show that transient labelling is fully

compatible with dynamic biomolecules by monitoring the conformational dynamics of a DNA Holliday Junction (HJ) using long-lived smFRET measurements. Our strategy can be easily tuned to adapt its temporal resolution and observation span to a plethora of biological systems and applications.

RESULTS

Design principles for REFRESH. Since the labelling of a target biomolecule (hereafter, the "target") is based on a series of reversible binding events, the resulting time-traces from a target will contain dark intervals; the ideal traces should have as few and as short dark intervals as possible, achieving a temporal target sampling that approaches 100 %. This aspiration for near-complete sampling creates two requirements: first, dark intervals due to r-label-exchange events (where a dissociated r-label is replaced by a new one) need to be short, and ideally should occur on a timescale similar (or shorter) than the exposure time of the single-molecule imaging experiment (typically, in the 20-200 ms range). Second, dark intervals due to any bleaching of an r-label while bound to the target need to be minimised both in number and duration.

To fulfil these requirements, we use the following set of strategies: (I) To achieve high on-rates, we optimise DNA sequences by avoiding intramolecular complementarity. (II) To minimize dark intervals, we employ high r-label concentrations, a condition facilitated by r-labels that, when unbound, remain in a dark, quenched state. (III) To increase the photobleaching lifetime of the fluorophore, we use a photo-stabilisation system. (IV) To ensure r-label dissociation *before* bleaching, we tune the off-rate of the r-label from the target. (V) To use the photon budget of each r-label efficiently, we maximise the binding time between r-label and target within the limit set by photobleaching.

Optimising hybridisation kinetics for REFRESH. Using a custom Hidden-Markov-Model (HMM) model, we determined suitable kinetic parameters for our r-labels (Figure 2A), which can occupy three states: bright (label hybridised and fluorescent), bleached (label hybridised but bleached, hence non-fluorescent), and unbound (label not hybridised). We visualised the sequences of states as simulated traces (Figure 2B) for a given set of on-, off-, and bleaching rates (k_{on}, k_{off}, and k_{bleach}, respectively); these rates determine the interconversion between states and can be tuned in the experimental setup.

The bleaching rate is ultimately limited by the laser power required for signal detection; using a laser power of 1.4 mW at 640 nm (the lower limit to ensure detectable spots on our microscope set-up), and with the employed photo-stabilisation, we observed a bleaching rate of $k_{bleach} = 0.02\ s^{-1}$ (Figure S2) for ATTO647N, the main fluorophore used in this work. Given that our design comprises two ATTO647N fluorophores (see later sections and *Methods*), the rate of both dyes bleaching is $k_{bleach,\ total} = |(k_{bleach})|^2\ s^{-1} = 0.0004\ s^{-1}$. From the simulations (for effects of the different parameters, see also Figure S1), we concluded that, to ensure the bleached state is short-lived, k_{off} has to be >25-fold larger

than $k_{bleach,\ total}$ (k_{off} >0.01 s^{-1}). Similarly, k_{on} should be ~25-fold larger than k_{off} (k_{on}> 0.25 s^{-1}, see Figure 2B).

To identify DNA sequences and lengths that led to the desired binding and unbinding rates, we calculated the kinetics for a set of sequences. To maximise the on-rates for a given length, we avoided interactions within the sequence by choosing just two non-complementary bases per sequence (e.g., only T and G). We hypothesised that in this case, and for a given salt concentration and temperature, only the G/C content and the DNA length will determine the binding kinetics. To outline the available parameter space, we thus calculated the interaction kinetics for ssDNAs of different lengths containing only A/T or G/C bases.

In our calculations, on- and off-rates for DNA hybridisation span large ranges (Figure 2C-D; calculated at 500 mM NaCl and 100 nM r-label at 25°C using an algorithm by Zhang et al[24] and Santa Lucia et al[25]). The on-rate strongly depends on the r-label concentration, with a 100 nM concentration resulting in rates of ~1 s^{-1} (Figure 2C). Off-rates vary across orders of magnitude depending on length and the G/C content of the sequence (Figure 2D). Following our design principles, we chose as our r-label an 11-mer with a relatively low G/C content (20-30 %). This would allow an on-rate of ~1 s^{-1} and an off-rate of $\approx 10^{-3}$-10^{-2} s^{-1}, values well within the frame established using HMM modelling. Importantly, our r-labels are considerably longer than the imager strands employed in super-resolution techniques, since we want to minimise dark intervals (which, in contrast, are necessary for achieving sub-diffraction resolution). The lower off-rates for the renewable labels ensure efficient use of the photon budget of the fluorophores employed.

Quenching strategy. To keep the dark intervals low, our technique relies on using high concentrations of unbound labels (100-500 nM, as in our simulations); this, in turn, leads to a significant fluorescence background that needs to be suppressed. A standard way to reduce the fluorescence background is through the use of an evanescent excitation field in a total-internal-reflection fluorescence (TIRF) microscope; however, this mode of microscope still cannot allow detection of single immobilised molecules in the presence of >50 nM of unbound label.[20–23]

To further suppress the fluorescence background, we considered a strategy for quenching the fluorescence of unbound labels. This strategy uses a short ssDNA labelled with two ATTO647N fluorophores (one on either end) that exhibit contact-mediated quenching in solution; when bound to the target, the state of quenching is lifted, leading to the appearance of fluorescence corresponding to two ATTO647N fluorophores.[20] Use of this quenching strategy improves the SNR further and effectively makes the r-label (as a unit) more photostable, since complete loss of fluorescence requires bleaching of both fluorophores and thus will require more time to occur.

To characterise the level of de-quenching associated with the target binding of the 2xATTO647N DNA, we performed ensemble fluorescence measurements that showed a 4-fold increase in fluorescence

intensity upon addition of an excess of complementary DNA (Figure S3). We also examined other single-molecule quenching approaches using dark quenchers[26] (our r-label sequence with a 3'-Dabcyl or Black-Hole-Quencher 3, and a 5'-ATTO647N), or two terminal ATTO655 dyes; these approaches were less successful, either due to lack of contact-mediated quenching (ATTO647N-DABCYL, or 2xATTO655; Figure S3), or due to more modest de-quenching upon target binding (ATTO647N-BHQ3; Figure S3).

To examine the performance of the de-quenched DNA while bound to the target, we examine renewable SMF time-traces of a bound target. We observe two fluorescence intensity levels, the lower of which matches the intensity observed for a single ATTO647N fluorescence and is at half the counts of the higher level (Figure 3). We attribute the lower level to a singly-labelled target (either due to bleaching or incomplete fluorophore incorporation during synthesis) and the higher level to the doubly-labelled target. The presence of the high level of ATTO647N fluorescence intensity also suggests that de-quenching upon target binding is complete, with no significant impact of any remaining contact-mediated quenching or homo-FRET processes on the quantum yield.

Near-continuous single-molecule fluorescence for hours using REFRESH. We first implemented our renewable strategy on a surface-immobilised DNA target containing a docking DNA strand complementary to our r-label, which was modified to implement the 2xATTO647N quenching strategy. The target was also labelled with a green Cy3B fluorophore, which served as a localisation signal. During the experiment, we first localised our target using the green emission channel (Figure 3A, left); we then added the r-label strands, and recorded movies under red excitation (Figure 3A, right), which were then used to generate time-traces.

We generated time-traces at r-label concentrations of 20, 100, and 200 nM (Figure 3B-D). At all concentrations, the fluorescence traces showed several intervals of high intensity, corresponding to a r-label being bound to the target (blue shading) followed by disappearance of the fluorescence signal (blue triangles), which we attribute to r-label dissociation (and *not* to bleaching, which would have led to a step-wise decrease in intensity due to the presence of two fluorophores per r-label). As expected, the dark intervals became shorter with increasing r-label concentration (compare Figure panel 3B with C and D), and for concentrations exceeding 100 nM, become negligible (<2 %). In some instances, bleaching of one fluorophore occurs, reducing the fluorescence signal by ~50 % (yellow shading); a further intensity decrease can be caused due to r-label unbinding or bleaching of the second fluorophore.

On average, we observe about 5-7 label-exchange events per 350 s of near-continuous traces, which result in an average bound time of 50-70 s, or an off-rate of $k_{off} \approx 0.02$ - $0.03\ s^{-1}$; notably, label exchanges occurring faster than the exposure time of 100 ms cannot be observed.

Since the observation time of a target is now almost immune to the photobleaching, we can monitor the target for much longer time-spans; we thus recorded continuous traces over one hour using 100 nM r-

label and an exposure time of 300 ms (Figure 4). The use of a longer exposure time (300 ms vs. 100 ms) was chosen to reduce file sizes and simplify data handling, and can be shortened to 100 ms (or less) if we need to resolve dynamic processes occurring faster than the 300-ms timescale. The traces (Figure 4) show, with the exception of just a few frames, a continuous signal over the complete time-span. The two intensity levels from double -or single-labelled r-labels can be clearly distinguished (≈400 vs ≈200 counts).

Interestingly, in the top trace in Figure 4, between minute 10 and 25, we almost exclusively observe the medium signal level (≈200 counts), along with two rapid label exchanges (where the signal count is zero, i.e., minutes 17 and 22). This observation indicates a significant presence of singly-labelled r-labels in solution, either through bleaching or incomplete synthesis. Further, the hour-long traces feature fewer exchange events and longer bound times than expected from extrapolating short traces, likely due to missing label exchanges that occur faster than 300 ms. An observation span of one hour is an improvement of two orders of magnitude over the bleaching time of individual ATTO647N fluorophores under our conditions ($t_{bleach} \approx 50$ s, see Figure S2).

Observation of conformational dynamics using REFRESH-FRET. We then moved to the experimental implementation of long-lived smFRET measurements using r-labels. As a model system, we chose a Holliday junction (HJ), a well-studied dynamic four-arm DNA structure that allows us to monitor repeated interconversions between two conformational states distinguishable using FRET.[27]

We first assembled a "standard" HJ by using four 22 nucleotide-long ssDNA strands, one of which carries a covalently attached FRET donor and a second carrying a covalently attached FRET acceptor; this labelling strategy results in the fluorophores appearing at the ends of two of the HJ's four arms (Figure 5A). In the two main HJ conformational states, the fluorophores are positioned at different distances from each other, resulting in two distinct FRET efficiencies (a high FRET state of ≈ 0.75 and a low FRET state of ≈ 0.25).

To monitor both FRET and fluorophore stoichiometries, we used alternating-laser excitation (ALEX) of the immobilised molecules using 200-ms frame times. For each ALEX frame (see *Methods*), the AA signal reports on the presence of the acceptor, and the DD and DA signals are used to observe FRET and conformational changes. Figure 5B shows a representative example of a fluorescence trace recorded from the reference HJ: the AA trace shows fluctuations between two spectral states of ATTO647N, which have been described before.[28] On the other hand, DD and DA show anti-correlated fluctuations indicating dynamic FRET processes, which are also reflected in the apparent FRET efficiency (E) trace (bottom panel), which shows transitions between high (E ≈ 0.75) and low (E ≈ 0.25) values.

To implement REFRESH-FRET, we extended the strand carrying the acceptor by a docking strand complementary to our r-label. In solution, we provide the self-quenching r-labels which bind to the

docking strand (Figure 6A). In the two main HJ conformational states, the fluorophores are again positioned at different distances from each other, resulting in two distinct FRET efficiencies.

We then examined the dynamics of this HJ (Figure 6) using ALEX and extracted time traces. This time, the AA trace specifically reports on the presence of the r-label. With the exceptions of very few frames, the AA signal is continuous over the recorded period at an r-label concentration of 100nM. As seen in the zoomed-in segment in Figure 6B, fluctuations in the DD and DA channels (top) are anti-correlated, indicating FRET dynamics, which result in the E value showing clear transitions between high ($E \approx 0.75$) and low ($E \approx 0.25$) values.

We then analysed the E traces (see *Methods*) to generate FRET efficiency frequency distributions and dwell-time histograms for the HJ as measured using standard smFRET (Figure 7A and C) and as measured using REFRESH-FRET (Figure 7B and D). Both structures show similar FRET distributions, with peaks at E values of ≈ 0.25 and ≈ 0.75. The relative abundance of the two fractions for the HJ (reference: low FRET: ≈ 73 % high FRET: ≈ 27 %, REFRESH: low FRET: ≈ 56-58 %, high FRET: ≈ 42-44 %) indicate a $K_{high\ ->\ low}$ of ≈ 2.7 and ≈ 1.2-1.4 (reference HJ and REFRESH-FRET HJ, respectively). This indicates that the low-FRET state is energetically slightly favoured in both structures, however the difference between the states is ~ 2-fold smaller when using r-labels.

We also determined the kinetic constants for the interconversions at three r-label concentrations (20, 100, and 200 nM), which showed remarkable consistency (see Figure 7D and S4C-D). At 100 nM, the rates were $k_{high->low} = 4.00 \pm 0.15\ s^{-1}$ and $k_{low->high} = 2.44 \pm 0.17\ s^{-1}$, equating to a $K_{high->low} \approx 1.6$. The reference HJ had a $k_{high->low} = 5.51 \pm 0.22\ s^{-1}$, $k_{low->high} = 1.61 \pm 0.04\ s^{-1}$ or a $K_{high->low} \approx 3.4$. These values agree well with the values obtained from the population fitting and further show that the shift in equilibrium when comparing reference and REFRESH HJ is mainly due to a stabilisation of the high FRET state. An interconversion constant $K_{high->low}$ near unity is consistent with previously published literature on the HJ (Gilboa et al found a $K_{high->low}$ of ≈ 3.7, McKinney et al report a $K_{high->low}$ of ≈ 1 across different [$MgCl_2$]; Ref. [27,29]).

Our results clearly establish that we can use REFRESH-FRET to resolve conformational dynamics well below the second timescale over very long observation spans, whilst recovering the same FRET efficiencies as our reference structure.

DISCUSSION

We have shown that we can perform hour-long continuous observations of the presence and dynamics of single immobile biomolecules using renewable labelling based on the hybridisation of short, ssDNA labels. This was enabled by tuning the processes of binding and unbinding of our r-labels to achieve continuous fluorescence traces. With our designed r-label sequence, near-continuous fluorescence traces could be observed for more than 1h, substantially longer than for equivalent stably bound fluorescent

labels under the same conditions. Importantly, due to constant r-label exchange, the trace length is not limited by the bleaching of individual fluorophores. Since the label replacement happens on the timescale of our exposure time, the fluorescence signal is only lost for very few frames at a time, and we can achieve a temporal target sampling of >98%. Overall, REFRESH allows us to observe traces with 100 ms resolution over hours, covering timescales over five orders of magnitude.

Exchanging bleached fluorescent labels with fresh ones has been explored previously for self-healing and regeneration of DNA-Nanostructures,[30] where an incubation with fresh staple strands restored a variety of damages, amongst them photo-damage to fluorescently labelled staples. A real-time exchange of fluorescent labels for bleaching-free labelling has also very recently been shown by Vermeer et al.,[31]; however, since the reported temporal target sampling was ~50% per probe, this approach does offer continuous observations. In another approach to achieve continuous fluorescence signals over time spans of about 1h, Stehr et al. also used an array of six binding sites for transient DNA labels and optimised binding/unbinding kinetics to allow single-particle tracking for hours.[32] While this approach is attractive for SMF measurements with a single fluorophore (since it can operate at lower label concentrations), it is not compatible with smFRET studies, since the use of multiple fluorophores along the DNA strand used for labelling will create a complex and uninterpretable web of fluctuating photophysical interactions between many potential FRET donor and acceptors.

Compatibility of smFRET with renewable labelling. Our studies on the dynamic HJ show conformational dynamics with kinetics that are independent of r-label concentrations. The interconversion rates for the REFRESH-FRET HJ were also in good agreement with the results obtained on the covalently labelled HJ, although some stabilisation of the high-FRET state (~2-fold) was observed in the REFRESH-FRET cases.

Further, the FRET efficiencies for the two states are similar, which validates the choice of the fluorophore location on the r-label. In general, the fluorophore should be positioned as closely as possible to the point of the docking strand attachment to minimise any uncertainty in the distance measurement due to motions of the fluorophore on the target; however, for some systems, it may be advantageous to allow some flexibility in the attached r-label by the addition of a few linker bases.

The current design operates at 100 nM r-label and 100-ms exposures. To resolve faster processes, shorter exposures can be enabled by increasing the excitation power and using shorter r-labels at higher concentrations; currently, concentrations of up to 500 nM are feasible using quenching of unbound r-labels carrying two ATTO647N fluorophores[20]. In our traces, we also see binding of a single-labelled r-label (e.g., see top trace in Figure 4), which suggests the presence of a significant proportion of non-quenched labels in the buffer, caused either by incomplete synthesis and separation of single- from double-labelled r-labels, or by bleaching of unbound r-labels whilst illuminated on the microscope. Since both sources of background can be addressed experimentally (by further purifying the r-label after

synthesis, and implementing constant buffer exchange through microfluidics), we should be able to extend the range of operational r-label concentrations.

Extensions of single-molecule fluorescence via renewable labelling. Here, we have implemented a FRET assay using a covalently attached donor dye (Cy3B), and an r-label carrying the acceptor ATTO647N. For hour-long FRET observations, the donor can also be provided as an r-label, albeit using an orthogonal sequence to that of the acceptor r-label in order to ensure site-specific binding. To quench unbound donor r-labels, we envision a strategy akin to that in DNA-PAINT combinations with fluorogenic 'imagers' [33]: due to high FRET-quenching even in the hybridised state, the use of dye-dark quencher pairs on short r-labels (in our work, 11 nt) or imagers (commonly 6-9 nt) is unfavourable (see Figure S3). Chung et al extended the imager length to 15 nt and used mismatches between imager and docking strand to reduce bound times to allow for blinking and super-resolution imaging.[33] Using 15-nt long ssDNA r-labels for the donor exchange, we expect similar binding kinetics as our established acceptor r-label, and thus enable hour-long continuous FRET observations.

We further envision to use REFRESH on proteins or nucleic acids. To allow for site-specific labelling of proteins with our docking strand, several strategies have been established. Small proteins can be labelled using cysteine chemistry; since they naturally contain only few cysteines, they can be mutated so that only one is accessible to linking reactions and can be labelled specifically. For larger proteins, which often contain multiple cysteines stabilising secondary structures, site-specific labelling strategies to link them to short ssDNAs include use of tags, such as hexahistidine-, Halo- or SNAP-tags.[34,35]

For REFRESH-FRET experiments, two orthogonal docking strands need to be placed on the protein of interest. This can be achieved by labelling two surface-exposed cysteines stochastically, and identifying the correctly labelled molecules via their fluorescence stoichiometry. Further, site-specific labelling could be achieved using unnatural amino acids like 4-azido-phenylalanine, which can be incorporated via a repurposed STOP-codon and then attached to the docking strand via a Staudinger-Bertozzi ligation.[36] For multi-subunit protein complexes, various subunits could be labelled separately, before the whole protein is reconstituted to ensure specific labelling of individual sites.[36]

Ultimately, the observation time span is limited by the survival time of the target molecule, especially the docking strand. In DNA-PAINT, photo-destruction of docking strands has been reported; however, DNA-PAINT uses 10-25-fold higher laser powers than in our experiments.[37] Additionally, DNA-PAINT experiments are often performed without photo-stabilisation, which both preserves fluorescent dyes and prevents damage to DNA structures[30] (such as docking sites or r-labels). Consistent with this, we have observed only a few traces (<5%) which permanently enter a dark state after some time (or show significant reduced on-times).

In our renewable labelling strategy, we have used a photo-stabilisation system based on glucose oxidase and TROLOX; however, this is known to decrease pH over time (≈30 min)[38]. To prolong this process,

alternative stabilisation systems such as the pyranose oxidase system[39] can be used. Alternatively, one can use microfluidics to implement a constant buffer exchange and replenish unbleached, free r-labels.

Long observation spans create challenges for smooth data acquisition and analysis. Lateral drift of the sample after several minutes on the microscope can become noticeable; hence, un-drifting, either using the images themselves or aided by fiducial markers will be useful.

Future applications. REFRESH allows monitoring processes at high temporal resolution over long observation spans, opening many new opportunities for single-molecule studies, as outlined below.

Access long-lived conformational states in complex proteins. Recent studies indicate the presence of protein conformational changes occurring at timescales inaccessible to standard smFRET due to photobleaching. REFRESH-FRET will allow monitoring of these changes without sacrificing temporal resolution. An attractive target for such studies is the bacterial RNA polymerase (RNAP), for which an important structural module, the RNAP clamp, is conformationally flexible within the 1-s timescale. It has been shown, however, that many RNAP molecules appear static over typical observation spans (~10 s).[40,41] Intriguingly, these static molecules can switch to a specific conformational state upon addition of substrate DNA, suggesting that they undergo conformational switching at timescales inaccessible under current smFRET measurements. Such slow conformational changes may have substantial functional relevance, as proposed for protein machines such as the RecBCD DNA helicase.[42]

Access rare states and slow reactions. Bleaching-limited single-molecule experiments may not provide enough data points to identify rare states or transitions; however, such rare states may be key to many mechanisms and define rate-limiting steps. Using renewable fluorescence, processes can be monitored across many steps or reaction cycles, allowing the collection of large data-sets and statistics on rare states, thus helping to identify their functional significance and reconstruct complex energy landscapes.

Perform repeated observations on the same molecule. Renewable labelling allows observation of the *same* molecule through multiple rounds of its activity, e.g., the same RNAP molecules can be monitored during several rounds of transcription of the same or different promoter DNA sequences, or in the presence of other molecules (e.g., antibiotics, transcription factors) which may alter RNAP behaviour. Further, using multiple docking strands on a target molecule, we can detect different FRET pairs in subsequent observation rounds, monitoring multiple distances on the same molecule.

Perform long observations of a substrate through several rounds of processing. Renewable fluorescence also allows monitoring of an appropriate substrate as it is recognised or processed by different proteins; for example, we envision systems that detect the repeated synthesis and/or degradation of specific RNA molecules both *in vitro* and *in vivo* using transient fluorescent in situ hybridization (FISH).[43–46] Importantly, the reversible nature of renewable labelling would permit interactions with RNA-processing proteins without the interference caused by stably bound FISH probes.

METHODS

Simulation of imaging processes in an HMM model. MATLAB provides an in-built HMM modelling and decoding tool, which generates sequences of system states, observed states, and output probabilities of these observed states. These were interpreted as pseudo-single molecule fluorescence intensity traces.

The input parameters of the model consist of a transition probability matrix T, reflecting the kinetic behaviour of the system (determined by the transition rates), and an emission probability matrix E which maps the likelihood of a specific observed state i (on or off), given a system state j (bleached, unbound, or bright). For the model, we assumed that the transition rates k_{off} and k'_{off} to be the same and are both reflected by n_{off} (see Figure 2A).

$$T = \begin{array}{c} \\ bleached \\ unbound \\ bright \end{array} \begin{array}{c} \begin{array}{ccc} bleached & unbound & bright \end{array} \\ \begin{bmatrix} 1-n_{off} & n_{off} & 0 \\ 0 & 1-n_{on} & n_{on} \\ n_{bleach} & n_{off} & 1-n_{off}-n_{bleach} \end{bmatrix} \end{array}$$

$$E = \begin{array}{c} \\ bleached \\ unbound \\ bright \end{array} \begin{array}{c} \begin{array}{cc} on & off \end{array} \\ \begin{bmatrix} 0.05 & 0.95 \\ 0.05 & 0.95 \\ 0.95 & 0.05 \end{bmatrix} \end{array}$$

Upon testing the script, the output is not very sensitive to changes in E, as long as it is still assumed that the actual hybridisation process is the dominant source of the observed signal.

Predicting Hybridisation kinetics. For this model, DNA hybridisation is assumed to be a reaction in equilibrium of association and dissociation according to the following reaction equation:

$$\text{rDNA} + \text{dDNA}_{comp} \rightleftharpoons \text{dsDNA}$$

rDNA is a short ssDNA oligo which freely diffuses in solution (r-label), $dDNA_{comp}$ is a surface-immobilised, complementary ssDNA oligo (docking strand). There is experimental evidence to suggest that the process also involves a parallel pathway leading to partially hybridised intermediates.[24,47] An overall three-state system with more rate constants would thus provide greater accuracy. Since, for our purposes, it is not important to distinguish the partially and the fully hybridised states, we decided to use the simpler two-state model.

In a first approximation, the hybridisation follows the Langmuir adsorption model, which describes the adsorption of ideal gasses onto surfaces in isothermal conditions. The underlying conditions formulated for the Langmuir model apply reasonably well to the adsorption of rDNA onto the surface covered in dDNA.[48]

As such, the hybridisation follows first-order reaction kinetics, associated with an elementary reaction constant, $k_{on,M}$. The dissociation is a zeroth-order reaction with a reaction constant k_{off}. The dissociation constant K_d for the reaction in thermodynamic equilibrium can be calculated according to equation (1):

$$K_d = k_{off}/k_{on,M} \quad (1)$$

K_d is linked to the free energy ΔG of the reaction, bridging the kinetics to the thermodynamics of the system (in equilibrium) according to equation (2):

$$K_d = e^{-\Delta G/(RT)} \quad (2)$$

where T is the temperature (K) and R is the universal gas constant (8.314 $JK^{-1}mol^{-1}$). The thermodynamics of the system are determined by reaction conditions (temperature, buffer composition) and reaction components (e.g., DNA sequence).

DNA hybridisation kinetics were calculated using an algorithm presented by Zhang et al.[24] The hybridisation rate predicted by this experimental model is equivalent to the rate constant of DNA-binding ($k_{on,M}$). The free energy ΔG of the hybridisation reaction was determined for the same temperature and salinity based on Santa Lucia et al.[25] The dissociation constant K_d is calculated from ΔG according to equation (2).

In a next step, the unbinding rate k_{off} is determined according to equation (3):

$$K_d = k_{off}/k_{on,M} \leftrightarrow k_{off} = K_d \cdot k_{on,M} \quad (3)$$

Holliday Junction annealing and immobilisation on surfaces Oligos were obtained from Metabion and Merck, dissolved to a final concentration of 100 µM and stored at -20ºC (for Sequences, see table S1). HJ components (strands: HJ-H, HJ-B, HJ-X, HJ-R or HJ-RI) were mixed in annealing buffer (200 mM Tris–HCl pH 8.0, 500 mM NaCl, 1 mM EDTA) at 2-4 µM, and then annealed in a thermocycler (program: heating to 90°C, then cooling to 25°C at 2°C/min, storing at 4°C).
HJs were immobilised via a biotinylated H-strand binding NeutrAvidin on coverslips coated by polyethylene-glycol (PEG). In wells of silicone gaskets, 20 µl of the HJs (100 pM-500 pM) were incubated for 10-30 s, followed by washing three times with 200 µl PBS. Subsequently, 40 µl of DNA imaging buffer (0.2 M $MgCl_2$, 50 mM HEPES pH 7.4, 6 mM BSA, 3 mM TROLOX, 1% Glucose, 40 µg/ml catalase and 0.1 mg/ml glucose oxidase) containing the stated r-label concentrations were added.

Movie Acquisition: Single-molecule fluorescence movies were collected using the Nanoimager-S single-molecule fluorescence microscope (Oxford Nanoimaging). The microscope was used as a widefield single-molecule fluorescence microscope with objective-based total internal reflection fluorescence (TIRF) illumination mode, with the excitation angle set at 53.6°. We performed the imaging using continuous-wave excitation (532 nm for Cy3B and 640 nm for ATTO647N) or alternating laser excitation (ALEX) mode, with the laser powers of 12 % or 2.9 mW at 532 nm; and 6 % or 1.4 mW at 640 nm. In all experiments, we used 100-ms exposures, apart from the 1 h time trace where 300 ms exposures were used to limit the size of files created.

Data Analysis: Movies were corrected for lateral drift as follows: localisations were found using Picasso[49] 'localize' and were then loaded in 'render' and un-drifted by RCC. The created drift file was used in a custom MATLAB (MathWorks) script to un-drift individual frames, which were then combined using FIJI.[50]

For all data except the 1-hr trace, fluorescence intensity vs. time traces were extracted and background-corrected using TwoTone.[51] The program extracts the fluorescence intensity in the green and red channel upon green excitation (DD and DA, respectively), and in the red channel upon red excitation (AA). Traces were manually inspected and any traces in which multiple molecules were detected, were discarded.

For one-colour experiments, the DD signal was used for localisation, and the AA signal was plotted as intensity vs time traces. In FRET experiments, all three signals were used to calculate the apparent FRET efficiency E and donor-acceptor stoichiometry S were calculated as follows:[52]

$$E = DA/(DD+DA) \quad (4)$$

$$S = (DA + DD)/(DD+DA+AA) \quad (5)$$

Two-dimensional E-S plots were used to select data points which contain both donor and acceptor dyes, for which E histograms were plotted.

Further analysis and HMM fitting were performed using ebFRET.[53] We fitted two distinct FRET states and extracted dwell time histograms for each state. By fitting these with a single exponential, the transition rates were determined. Stated rates with errors are means and standard deviations, respectively, of three independent experiments. The figures show exemplary data from one experiment per condition.

Because of the large file size, the above-mentioned extraction methods for fluorescence-vs-time traces were not available; 1-hr traces were thus extracted and background-subtracted manually using FIJI. Absolute count numbers between traces from TwoTone and FIJI are not directly comparable because different background subtraction processes were performed.

All traces and histograms were plotted using Origin (OriginLab).

Ensemble Fluorescence Measurements: For fluorescence spectra measurements, r-label strands were mixed in 100 µL buffer (50 mM HEPES, pH 7.4; 200 mM $MgCl_2$, 10 mM NaCl, 0.1 % BSA) to a final concentration of 100 nM. Fluorescence spectra were obtained at a scanning spectrofluorometer (PTI) using 1-s integration time per 1 nm wavelength intervals. Complementary DNA was added stepwise to achieve different concentrations (0.1-10 µM). Samples were excited at 620 nm (containing ATTO647N) or 640 nm (containing ATTO655).

Absorption spectra were measured at the NanoDrop absorption spectrometer (Thermo Scientific) with r-label concentrations of 1 μM in H_2O. Spectra were normalised to absorption at 260 nm to account for any variations in concentration.

Reference spectra of pure dyes are not to scale and were provided by ATTO-Tech.[54]

ACKNOWLEDGEMENTS. We thank Christof Hepp for critical reading of the manuscript, and the MICRON Advanced Bioimaging Facility (supported by Wellcome Strategic Awards 091911/B/10/Z and 107457/Z/15/Z) for access to a Nanoimager microscope in their facilities. This work was supported by the Wellcome Trust (110164/Z/15/Z to A.N.K.), the UK BBSRC (BB/R008655/1 to A.N.K.), a UK EPSRC studentship (project 2440758 to M.K.), and a doctoral fellowship of the Boehringer Ingelheim Fonds (to M.K.). The illustrations in Figures 1, 2A, 3A, and 5A-B were created using BioRender.com

CONFLICT OF INTEREST STATEMENT. The work was performed using miniaturised commercial microscopes from Oxford Nanoimaging, a company in which A.N.K. is a co-founder and shareholder.

References

1. Miller, H., Zhou, Z., Shepherd, J., Wollman, A. J. M. & Leake, M. C. Single-molecule techniques in biophysics: a review of the progress in methods and applications. *Reports on Progress in Physics* **81**, 24601 (2017).

2. Bruchez, M., Moronne, M., Gin, P., Weiss, S. & Alivisatos, A. P. Semiconductor Nanocrystals as Fluorescent Biological Labels. *Science (1979)* **281**, 2013–2016 (1998).

3. Kapanidis, A. N. & Weiss, S. Fluorescent probes and bioconjugation chemistries for single-molecule fluorescence analysis of biomolecules. *Journal of Chemical Physics* **117**, 10953–10964 (2002).

4. Löschberger, A., van de Linde, S., Dabauvalle, M.-C., Rieger, B., Heilemann, M., Krohne, G. & Sauer, M. Super-resolution imaging visualizes the eightfold symmetry of gp210 proteins around the nuclear pore complex and resolves the central channel with nanometer resolution. *Journal of Cell Science* **125**, 570–575 (2012).

5. Hess, S. T., Girirajan, T. P. K. & Mason, M. D. Ultra-High-Resolution Imaging by Fluorescence Photoactivation Localization Microscopy. *Biophysical Journal* **91**, 4258–4272 (2006).

6. Betzig, E., Patterson, G. H., Sougrat, R., Lindwasser, O. W., Olenych, S., Bonifacino, J. S., Davidson, M. W., Lippincott-Schwartz, J. & Hess, H. F. Imaging Intracellular Fluorescent Proteins at Nanometer Resolution. *Science (1979)* **313**, 1642–1645 (2006).

7. Pertsinidis, A., Zhang, Y. & Chu, S. Subnanometre single-molecule localization, registration and distance measurements. *Nature* **466**, 647–651 (2010).

8. Rust, M. J., Bates, M. & Zhuang, X. Sub-diffraction-limit imaging by stochastic optical reconstruction microscopy (STORM). *Nature Methods* **3**, 793–796 (2006).

9. Gelles, J., Schnapp, B. J. & Sheetz, M. P. Tracking kinesin-driven movements with nanometre-scale precision. *Nature* **331**, 450–453 (1988).

10. Schmidt, T., Schutz, G. J., Baumgartner, W., Gruber, H. J. & Schindler, H. Imaging of single molecule diffusion. *Proceedings of the National Academy of Sciences* **93**, 2926–2929 (1996).

11. Hellenkamp, B., Schmid, S., Doroshenko, O., Opanasyuk, O., Kühnemuth, R., Rezaei Adariani, S., Ambrose, B., Aznauryan, M., Barth, A., Birkedal, V., Bowen, M. E., Chen, H., Cordes, T., Eilert, T., Fijen, C., Gebhardt, C., Götz, M., Gouridis, G., Gratton, E., Ha, T., Hao, P., Hanke, C. A., Hartmann, A., Hendrix, J., Hildebrandt, L. L., Hirschfeld, V., Hohlbein, J., Hua, B., Hübner, C. G., Kallis, E., Kapanidis, A. N., Kim, J. Y., Krainer, G., Lamb, D. C., Lee, N. K., Lemke, E. A., Levesque, B., Levitus, M., McCann, J. J., Naredi-Rainer, N., Nettels, D., Ngo, T., Qiu, R., Robb, N. C., Röcker, C., Sanabria, H., Schlierf, M., Schröder, T., Schuler, B., Seidel, H., Streit, L., Thurn, J., Tinnefeld, P., Tyagi, S., Vandenberk, N., Vera, A. M., Weninger, K. R., Wünsch, B., Yanez-Orozco, I. S., Michaelis, J., Seidel, C. A. M., Craggs, T. D. & Hugel, T. Precision and accuracy of single-molecule FRET measurements—a multi-laboratory benchmark study. *Nature Methods* **15**, 669–676 (2018).

12. Ha, T., Enderle, T., Ogletree, D. F., Chemla, D. S., Selvin, P. R. & Weiss, S. Probing the interaction between two single molecules: fluorescence resonance energy transfer between a single donor and a single acceptor. *Proceedings of the National Academy of Sciences* **93**, 6264–6268 (1996).

13. Shashkova, S. & Leake, M. C. Single-molecule fluorescence microscopy review: shedding new light on old problems. *Biosci Rep* **37**, BSR20170031 (2017).

14. Hirschfeld, T. Quantum efficiency independence of the time integrated emission from a fluorescent molecule. *Appl. Opt.* **15**, 3135–3139 (1976).

15. Ha, T. & Tinnefeld, P. Photophysics of fluorescent probes for single-molecule biophysics and super-resolution imaging. *Annu Rev Phys Chem* **63**, 595–617 (2012).

16. Sharonov, A. & Hochstrasser, R. M. Wide-field subdiffraction imaging by accumulated binding of diffusing probes. *Proceedings of the National Academy of Sciences* **103**, 18911–18916 (2006).

17. Jungmann, R., Steinhauer, C., Scheible, M., Kuzyk, A., Tinnefeld, P. & Simmel, F. C. Single-molecule kinetics and super-resolution microscopy by fluorescence imaging of transient binding on DNA origami. *Nano Lett* **10**, 4756–4761 (2010).

18. Jungmann, R., Avendaño, M. S., Woehrstein, J. B., Dai, M., Shih, W. M. & Yin, P. Multiplexed 3D cellular super-resolution imaging with DNA-PAINT and Exchange-PAINT. *Nature Methods* **11**, 313–318 (2014).

19. Spahn, C., Hurter, F., Glaesmann, M., Karathanasis, C., Lampe, M. & Heilemann, M. Protein-Specific, Multicolor and 3D STED Imaging in Cells with DNA-Labeled Antibodies. *Angewandte Chemie International Edition* **58**, 18835–18838 (2019).

20. Andrews, R., Steuer, H., El-Sagheer, A. H., Mazumder, A., el Sayyed, H., Shivalingam, A., Brown, T. & Kapanidis, A. N. Transient DNA binding to gapped DNA substrates links DNA sequence to the single-molecule kinetics of protein-DNA interactions. *bioRxiv* 2022.02.27.482175 (2022) doi:10.1101/2022.02.27.482175.

21. Peng, S., Wang, W. & Chen, C. Breaking the Concentration Barrier for Single-Molecule Fluorescence Measurements. *Chemistry – A European Journal* **24**, 1002–1009 (2018).

22. Holzmeister, P., Acuna, G. P., Grohmann, D. & Tinnefeld, P. Breaking the concentration limit of optical single-molecule detection. *Chem. Soc. Rev.* **43**, 1014–1028 (2014).

23. van Oijen, A. M. Single-molecule approaches to characterizing kinetics of biomolecular interactions. *Current Opinion in Biotechnology* **22**, 75–80 (2011).

24. Zhang, J. X., Fang, J. Z., Duan, W., Wu, L. R., Zhang, A. W., Dalchau, N., Yordanov, B., Petersen, R., Phillips, A. & Zhang, D. Y. Predicting DNA hybridization kinetics from sequence. *Nat Chem* **10**, 91–98 (2018).

25. SantaLucia, J. A unified view of polymer, dumbbell, and oligonucleotide DNA nearest-neighbor thermodynamics. *Proceedings of the National Academy of Sciences* **95**, 1460–1465 (1998).

26. le Reste, L., Hohlbein, J., Gryte, K. & Kapanidis, A. N. Characterization of dark quencher chromophores as nonfluorescent acceptors for single-molecule FRET. *Biophys J* **102**, 2658–2668 (2012).

27. McKinney, S. A., Déclais, A. C., Lilley, D. M. J. & Ha, T. Structural dynamics of individual Holliday junctions. *Nature Structural Biology* **10**, 93–97 (2003).

28. Vogelsang, J., Kasper, R., Steinhauer, C., Person, B., Heilemann, M., Sauer, M. & Tinnefeld, P. A reducing and oxidizing system minimizes photobleaching and blinking of fluorescent dyes. *Angewandte Chemie International Edition* **47**, 5465–5469 (2008).

29. Gilboa, B., Jing, B., Cui, T. J., Sow, M., Plochowietz, A., Mazumder, A. & Kapanidis, A. N. Confinement-free wide-field ratiometric tracking of single fluorescent molecules. *Biophys J* **117**, 2141–2153 (2019).

30. Scheckenbach, M., Schubert, T., Forthmann, C., Glembockyte, V. & Tinnefeld, P. Self-Regeneration and Self-Healing in DNA Origami Nanostructures. *Angewandte Chemie International Edition* **60**, 4931–4938 (2021).

31. Vermeer, B. & Schmid, S. Can DyeCycling break the photobleaching limit in single-molecule FRET? *Nano Research* (2022) doi:10.1007/s12274-022-4420-5.

32. Stehr, F., Stein, J., Bauer, J., Niederauer, C., Jungmann, R., Ganzinger, K. & Schwille, P. Tracking single particles for hours via continuous DNA-mediated fluorophore exchange. *Nature Communications* **12**, 4432 (2021).

33. Chung, K. K. H., Zhang, Z., Kidd, P., Zhang, Y., Williams, N. D., Rollins, B., Yang, Y., Lin, C., Baddeley, D. & Bewersdorf, J. Fluorogenic DNA-PAINT for faster, low-background super-resolution imaging. *Nature Methods* **19**, 554–559 (2022).

34. Schlichthaerle, T., Strauss, M. T., Schueder, F., Auer, A., Nijmeijer, B., Kueblbeck, M., Jimenez Sabinina, V., Thevathasan, J. v, Ries, J., Ellenberg, J. & Jungmann, R. Direct Visualization of Single Nuclear Pore Complex Proteins Using Genetically-Encoded Probes for DNA-PAINT. *Angewandte Chemie International Edition* **58**, 13004–13008 (2019).

35. Nieves, D. J., Hilzenrat, G., Tran, J., Yang, Z., MacRae, H. H., Baker, M. A. B., Gooding, J. J. & Gaus, K. tagPAINT: covalent labelling of genetically encoded protein tags for DNA-PAINT imaging. *Royal Society Open Science* **6**, 191268 (2019).

36. Chakraborty, A., Mazumder, A., Lin, M., Hasemeyer, A., Xu, Q., Wang, D., Ebright, Y. W. & Ebright, R. H. Site-Specific Incorporation of Probes into RNA Polymerase by Unnatural-Amino-Acid Mutagenesis and Staudinger–Bertozzi Ligation. in *Methods in Molecular Biology* vol. 1276 101–131 (Humana Press, 2015).

37. Blumhardt, P., Stein, J., Mücksch, J., Stehr, F., Bauer, J., Jungmann, R. & Schwille, P. Photo-induced depletion of binding sites in DNA-PAINT microscopy. *Molecules* **23**, 3165 (2018).

38. Shi, X., Lim, J. & Ha, T. Acidification of the Oxygen Scavenging System in Single-Molecule Fluorescence Studies: In Situ Sensing with a Ratiometric Dual-Emission Probe. *Analytical Chemistry* **82**, 6132–6138 (2010).

39. Swoboda, M., Henig, J., Cheng, H.-M., Brugger, D., Haltrich, D., Plumeré, N. & Schlierf, M. Enzymatic oxygen scavenging for photostability without pH drop in single-molecule experiments. *ACS Nano* **6**, 6364–6369 (2012).

40. Duchi, D., Mazumder, A., Malinen, A. M., Ebright, R. H. & Kapanidis, A. N. The RNA polymerase clamp interconverts dynamically among three states and is stabilized in a partly closed state by ppGpp. *Nucleic Acids Res* **46**, 7284–7295 (2018).

41. Mazumder, A., Wang, A., Uhm, H., Ebright, R. H. & Kapanidis, A. N. RNA polymerase clamp conformational dynamics: Long-lived states and modulation by crowding, cations, and nonspecific DNA binding. *Nucleic Acids Research* **49**, (2021).

42. Liu, B., Baskin, R. J. & Kowalczykowski, S. C. DNA unwinding heterogeneity by RecBCD results from static molecules able to equilibrate. *Nature* **500**, 482–485 (2013).

43. Zhang, Z., Revyakin, A., Grimm, J. B., Lavis, L. D. & Tjian, R. Single-molecule tracking of the transcription cycle by sub-second RNA detection. *Elife* **3**, (2014).

44. Batani, G., Bayer, K., Böge, J., Hentschel, U. & Thomas, T. Fluorescence in situ hybridization (FISH) and cell sorting of living bacteria. *Scientific Reports* **9**, 18618 (2019).

45. Silverman, A. P. & Kool, E. T. Quenched autoligation probes allow discrimination of live bacterial species by single nucleotide differences in rRNA. *Nucleic Acids Research* **33**, 4978–4986 (2005).

46. Skinner, S. O., Sepúlveda, L. A., Xu, H. & Golding, I. Measuring mRNA copy number in individual Escherichia coli cells using single-molecule fluorescent in situ hybridization. *Nature Protocols* **8**, 1100–1113 (2013).

47. Traeger, J. C. & Schwartz, D. K. Surface-Mediated DNA hybridization: effects of DNA conformation, surface chemistry, and electrostatics. *Langmuir* **33**, 12651–12659 (2017).

48. Masel, R. I. *Principles of adsorption and reaction on solid surfaces*. vol. 3 (John Wiley & Sons, 1996).

49. Schnitzbauer, J., Strauss, M. T., Schlichthaerle, T., Schueder, F. & Jungmann, R. Super-resolution microscopy with DNA-PAINT. *Nat Protoc* **12**, 1198 (2017).

50. Schindelin, J., Arganda-Carreras, I., Frise, E., Kaynig, V., Longair, M., Pietzsch, T., Preibisch, S., Rueden, C., Saalfeld, S., Schmid, B., Tinevez, J.-Y., White, D. J., Hartenstein, V., Eliceiri, K., Tomancak, P. & Cardona, A. Fiji: an open-source platform for biological-image analysis. *Nature Methods* **9**, 676–682 (2012).

51. Holden, S. J., Uphoff, S., Hohlbein, J., Yadin, D., le Reste, L., Britton, O. J. & Kapanidis, A. N. Defining the limits of single-molecule FRET resolution in TIRF microscopy. *Biophys J* **99**, 3102–3111 (2010).

52. Uphoff, S., Holden, S. J., le Reste, L., Periz, J., van de Linde, S., Heilemann, M. & Kapanidis, A. N. Monitoring multiple distances within a single molecule using switchable FRET. *Nature Methods* **7**, 831–836 (2010).

53. van de Meent, J.-W., Bronson, J. E., Wiggins, C. H. & Gonzalez, R. L. Empirical Bayes Methods Enable Advanced Population-Level Analyses of Single-Molecule FRET Experiments. *Biophysical Journal* **106**, 1327–1337 (2014).

54. ATTO-TEC GmbH. Atto647N product Information. *https://www.atto-tec.com/ATTO-647N.html* (2022).

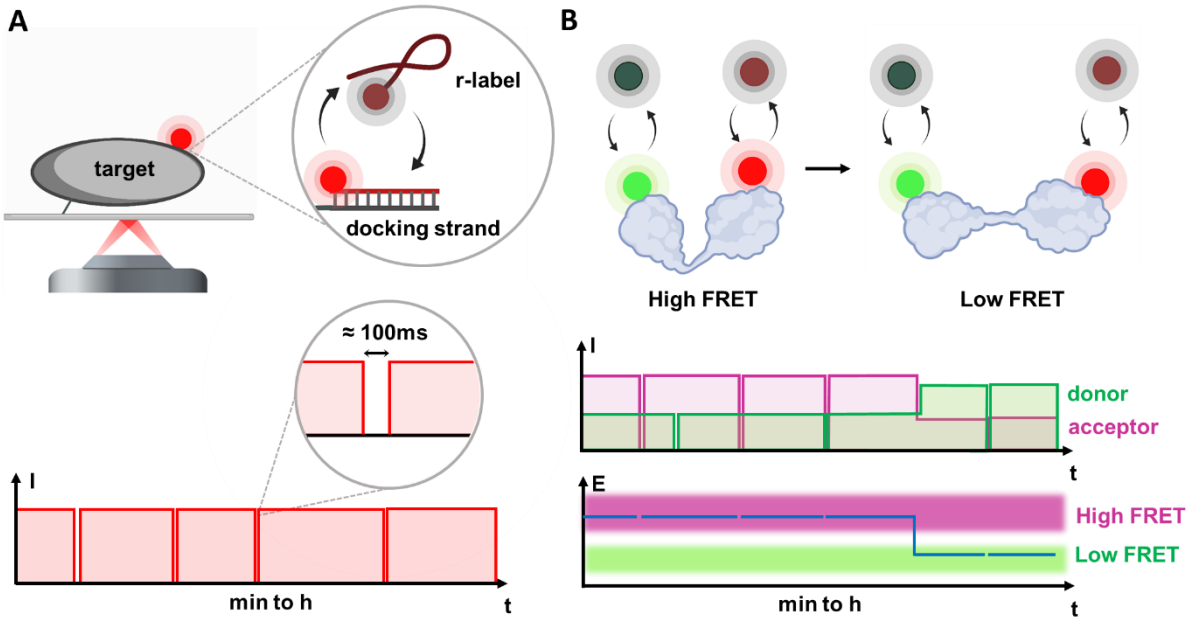

Figure 1: The principle of REFRESH. **A**. Continuous exchange is facilitated by transient hybridisation of short, ssDNA probes (r-labels) to complementary docking strands bound to a target molecule of interest (top). The schematic fluorescence trace (bottom) shows how, if intervals of exchange are short (below or on the order of the frame rate), a near- continuous fluorescence signal can be observed. **B**. REFRESH-FRET: The same labelling strategy is now applied to donor and acceptor dyes attached to a target of interest which undergoes conformational changes. The observed donor and acceptor traces (middle) can be used to calculate FRET efficiencies (bottom) and monitor conformational dynamics.

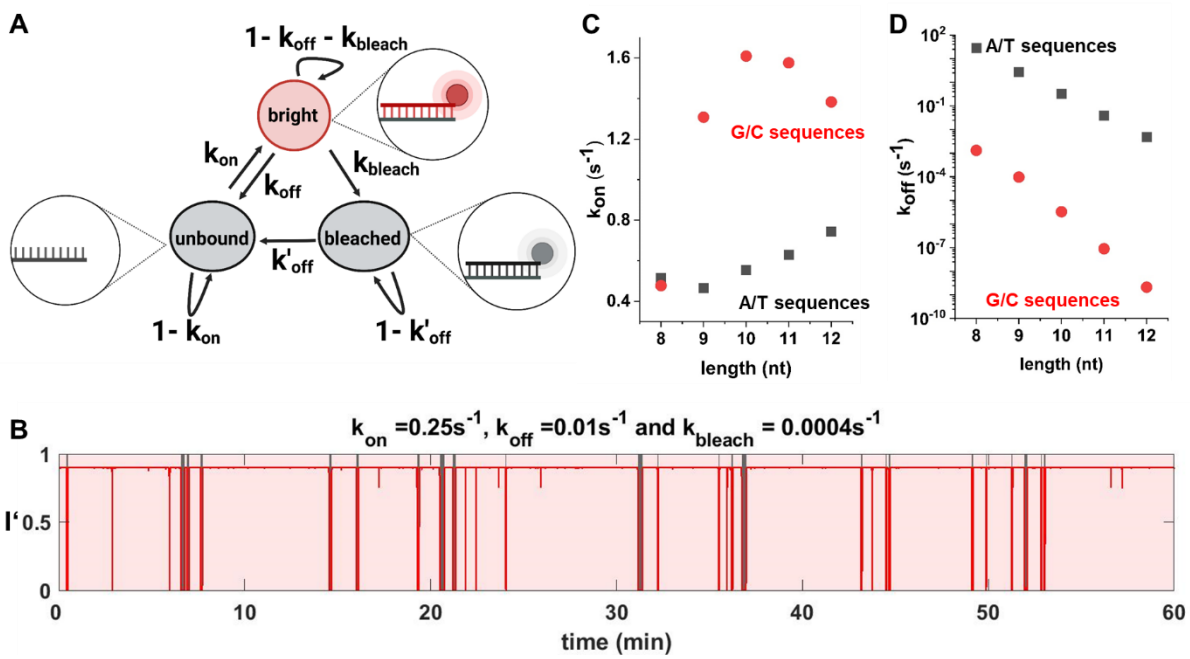

Figure 2: Simulations to find suitable kinetic parameters for the exchange. **A**. Markov-diagram of the process of r-label binding and unbinding in competition with photo-bleaching. **B**. Example of a simulated pseudo-intensity trace for optimised conditions. Red: Pseudo-intensity I', light red shading: bright state, dark grey shading: unbound state, light grey shading: bleached state (a clear example trace showing all three states can be seen in Figure S1). **C – D**. Calculated on- and off-rates for the hybridisation of short DNAs (at 100 nM) of different lengths and composition (either A/T only, or G/C only).

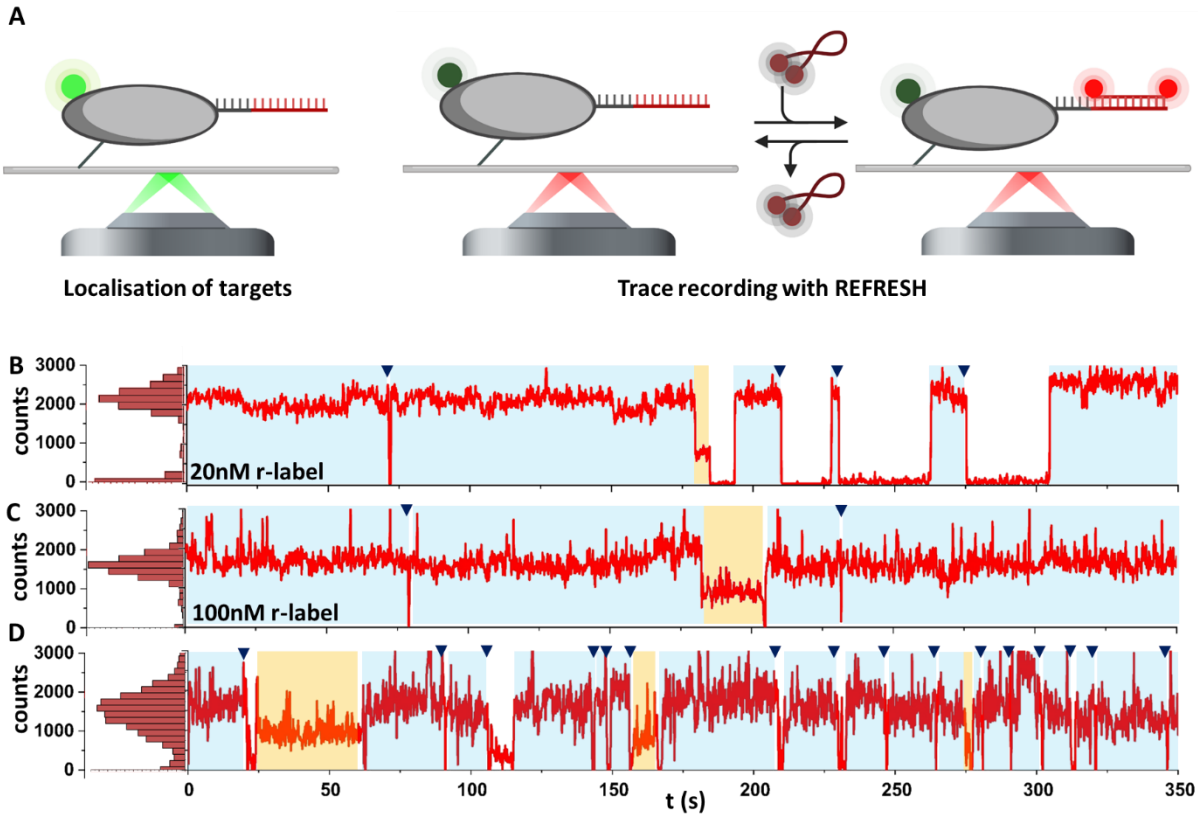

Figure 3: REFRESH allows for continuous fluorescence observations: **A**. Schematic of the experiment: the target molecule is localised on the surface via a Cy3B green label. After the addition of r-labels (carrying two ATTO647N), binding and unbinding can be observed at co-localising spots. **B-D**. Example traces at 20 nM (**B**), 100 nM (**C**), and 200 nM (**D**) r-label. The fluorescence traces repeatedly show intervals of high counts, corresponding to a fully labelled r-label strand being bound to the target (blue shading). The fluorescence is lost upon de-hybridisation (blue triangles). The intervals of low signals become shorter with increased r-label concentration (C vs. B vs. D); see also histograms on the left. In some instances, bleaching of one fluorophore occurs, reducing the fluorescence signal by 50% (yellow shading).

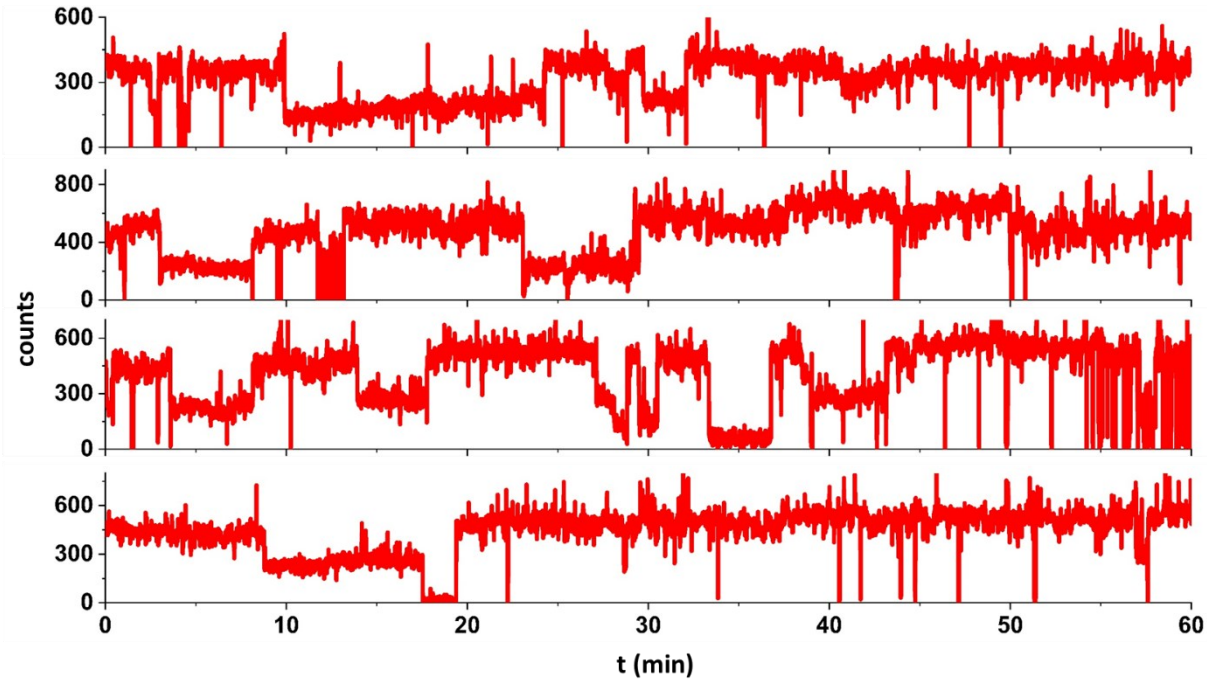

Figure 4: Fluorescence observations over hours: Selected example traces observed using 100 nM r-label over 60 min.

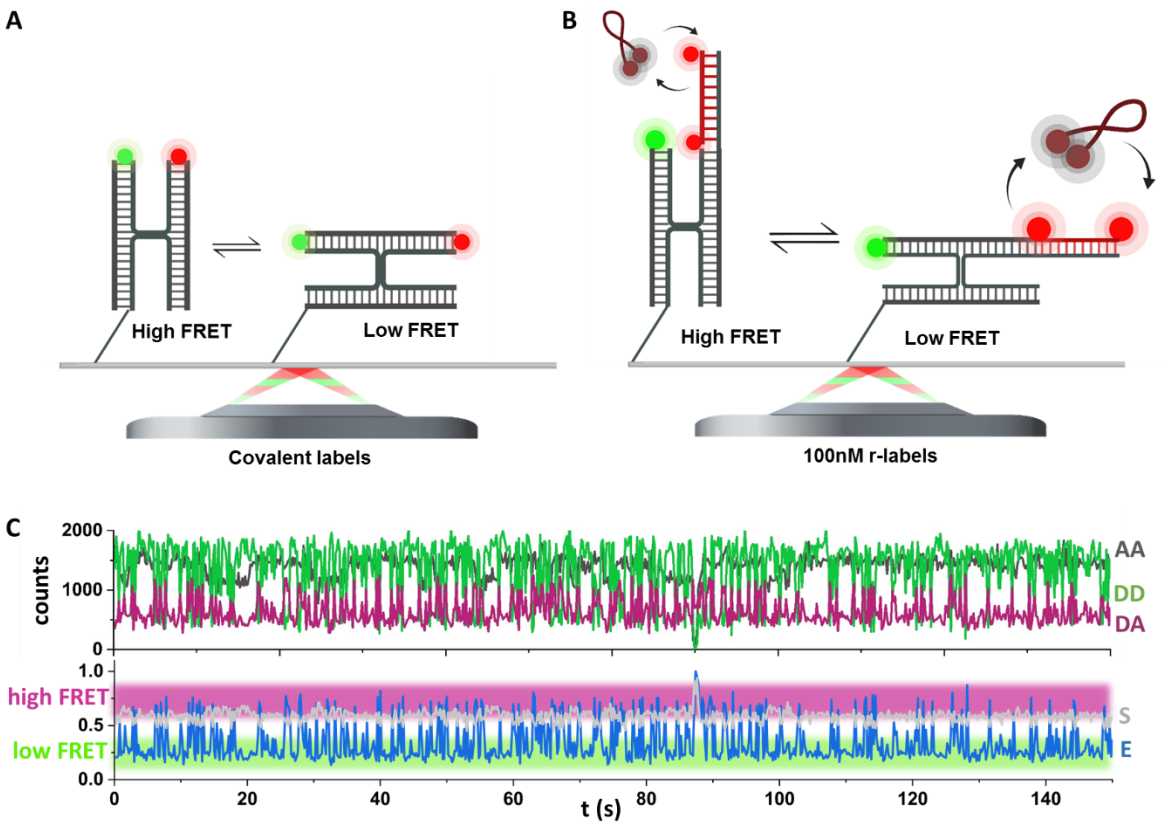

Figure 5: Observation of conformational dynamics using REFRESH-FRET. **A.** Reference structure of a covalently labelled HJ. **B.** HJ with exchanging acceptor label: The X-strand of the HJ carries a covalently attached Cy3B which serves as FRET donor, and an 11-bp extension on the R strand, which serves as binding site for the r-label. The r-label carries two ATTO647N dyes, at least one of which serves as FRET acceptor. **C.** Intensity-vs-time trace of the reference HJ with AA, DA, and DD signal (top), from which apparent FRET efficiency (E) and stoichiometry (S) were calculated. The anti-correlated fluctuations in DD and DA and the fluctuations in E indicated FRET dynamics between a high-FRET state ($E \approx 0.75$) and a low-FRET state ($E \approx 0.25$).

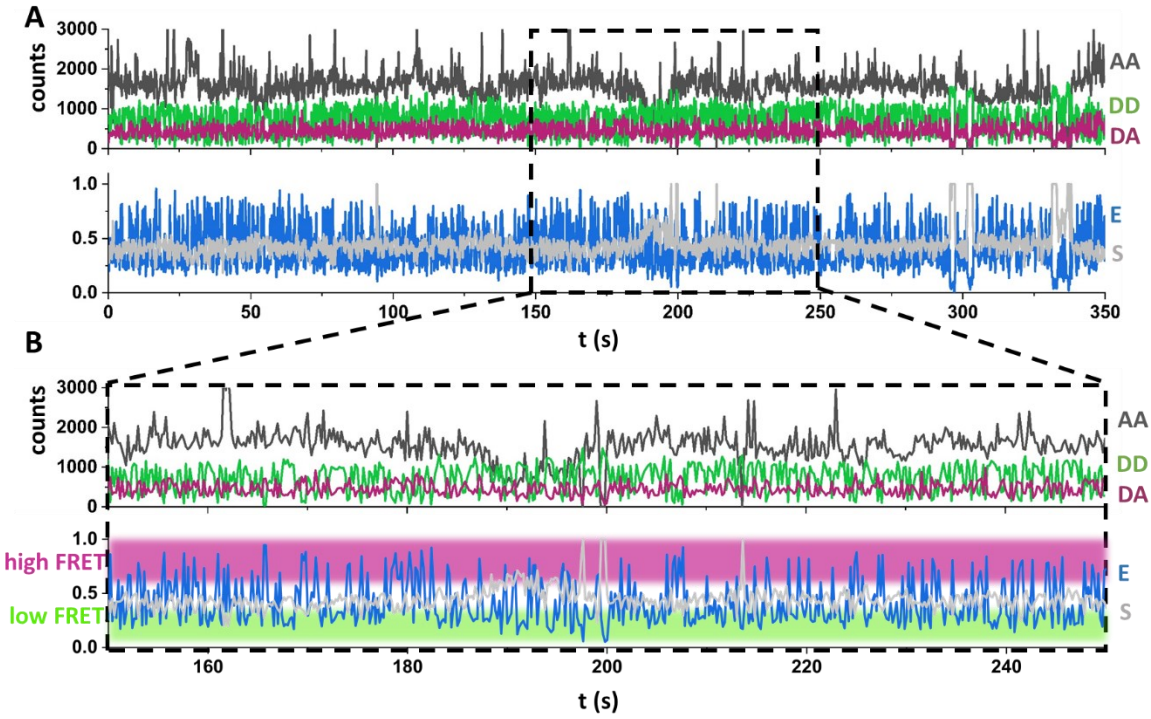

Figure 6: Exemplary traces observed on the REFRESH-HJ with 100 nM r-label. **A.** Full trace with AA, DD, and DA channel (top) and calculated FRET efficiency (E) and stoichiometry (S, bottom). **B.** Zoom-in of the trace in **A**. The anti-correlated fluctuations in the DD and DA channels (top) and the fluctuating E trace (bottom) indicate a dynamic interchange between a high-FRET state ($E \approx 0.75$) and a low-FRET state ($E \approx 0.25$).

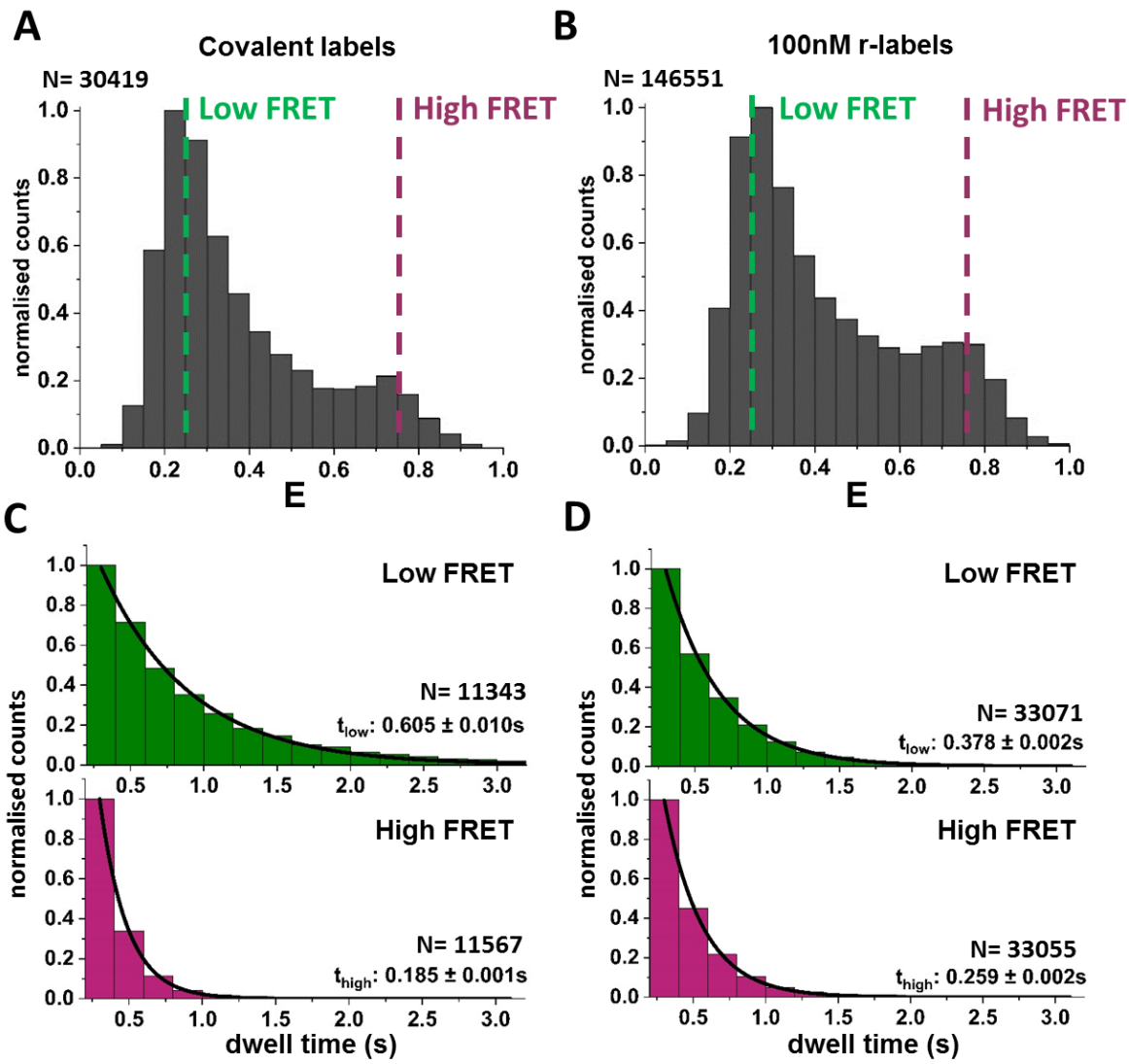

Figure 7: Monitoring conformational dynamics using REFRESH-FRET: Representative data from one experiment. **A-B.** FRET histograms of the reference HJ with covalent labels (**A**) and the HF with exchanging acceptor (**B**). **C –D.** Dwell time histograms of the high and low FRET states for the reference HJ (panel **C;** data from 64 molecules), and the HJ with exchanging acceptor label (**D**; data from 179 molecules), the errors stated are fitting errors.